High-power electro-optic switch technology based on novel transparent ceramic*

Xue-Jiao Zhang(张学娇)[1,2], Qing Ye(叶青)[1,†], Rong-Hui Qu(瞿荣辉)[1], and Hai-wen Cai(蔡海文)[1]

[1] *Shanghai Key Laboratory of All Solid-State Laser and Applied Techniques, Shanghai Institute of Optics and Fine Mechanics, Chinese Academy of Sciences, Shanghai* 201800, *China*

[2] *University of Chinese Academy of Sciences, Beijing* 100049, *China*

(Received 21 April 2015; revised manuscript received 22 December 2015; published online 18 January 2016)

A novel high-power polarization-independent electro-optic switch technology based on a reciprocal structure Sagnac interferometer and a transparent quadratic electro-optic ceramic is proposed and analyzed theoretically and experimentally. The electro-optic ceramic is used as a phase retarder for the clockwise and counter-clockwise polarized light, and their polarization directions are adjusted to their orthogonal positions by using two half-wave plates. The output light then becomes polarization-independent with respect to the polarization direction of the input light. The switch characteristics, including splitter ratios and polarization states, are theoretically analyzed and simulated in detail by the matrix multiplication method. An experimental setup is built to verify the analysis and experimental results. A new component ceramic is used and a non-polarizing cube beam splitter (NPBS) replaces the beam splitter (BS) to lower the ON/OFF voltage to 305 V and improve the extinction ratio by 2 dB. Finally, the laser-induced damage threshold for the proposed switch is measured and discussed. It is believed that potential applications of this novel polarization-independent electro-optic switch technology will be wide, especially for ultrafast high-power laser systems.

Keywords: switch, electro-optic switch, laser damage, optoelectronic material

PACS: 42.25.Hz, 42.79.–e, 42.70.Mp **DOI:** 10.1088/1674-1056/25/3/034202

1. Introduction

A high-power laser system with ultra-short pulse width and high average power has wide applications in modern material processing, military, space exploration, and medicine. Developing novel laser optoelectronic devices is a key for raising the current level of laser technology. An electro-optic switch using the electrically controllable refractive index modulation effect may realize a high switch speed (with response time of the order of nanoseconds or even picoseconds), which is very attractive for applications in the future all-optical network.[1] However, the fiber-type or waveguide structure limits the working area of available switch technologies, and their laser-induced damage thresholds are low, causing them unfit for use in the high-power laser systems. In order to develop high-power laser optoelectronic devices, some electro-optic crystals, such as potassium dihydrogen phosphate (KDP), lithium niobate ($LiNbO_3$), and barium metaborate (BBO) crystals, must be used. The KDP crystal possesses a large electro-optic coefficient, a high laser-induced damage threshold, and a large size via growth from solution. However, the deliquescent properties of the crystal require very strict application environments. The $LiNbO_3$ crystal has wide applications in optical communication and sensors because of its fast response time and low half-wave voltage; its low laser-induced damage threshold, however, restricts its usage in all-solid-state high-power laser modulation. Moreover, the polarization-dependent characteristic of the crystal is a significant destabilizing factor. The BBO crystal has an excellent damage threshold (> 20 GW/cm^2) in a high power density system, however, a driven voltage of tens-of-thousands volts is harsh for a working condition.[2–5]

Transparent electro-optic ceramics, i.e., lanthanum-modified lead zirconate titanate (PLZT) and lead magnesium niobate-lead titanite (PMNT), represent a class of materials possessing relaxor properties, which easily produce birefringences and exhibit good electro-optic effects. In general, the attractive features of PLZT and PMNT include a high electro-optic coefficient (approximately 100 times of that of $LiNbO_3$ at room temperature), a good optical transparency (larger than 95% with an antireflection film), a fast response time (about 100 ns), a large size (by the mature hot-pressing technique), and a high laser damage threshold. Especially for PMNT, a high electro-optic coefficient (2–5 times of that of the PLZT ceramic) and a low electric hysteresis (noticeably narrower in the range of 0–70 °C) have also been realized.[6–12] Therefore, these quadratic electro-optic ceramics may be adapted to high-power electro-optic components, especially in ultrafast laser applications.

In this paper, a novel high-power polarization-independent electro-optic switch technology based on these kinds of transparent quadratic electro-optic ceramics is proposed and analyzed both theoretically and experimentally.

*Project supported by the National Natural Science Foundation of China (Grant Nos. 61137004, 61405218, and 61535014).

†Corresponding author. E-mail: yeqing@siom.ac.cn

© 2016 Chinese Physical Society and IOP Publishing Ltd

The electro-optic ceramic is used as an electrically controllable phase retarder, which is inserted into a reciprocal structure Sagnac interferometer for the clockwise and counterclockwise polarized light. By adjusting the initial polarization states of two beams, a polarization-independent electro-optic switch technology is realized. The switch characteristics, including splitter ratio and polarization state, are analyzed and simulated in detail by the matrix multiplication method. An experimental setup is also built to verify the analysis results. Experimental findings agree with theoretical results. Finally, the laser-induced damage threshold of this proposed switch is also measured and discussed. It is believed that the novel polarization-independent electro-optic switch technology will have wide potential applications in the fields of the ultrafast high-power laser systems.

The rest of this paper is organized as follows. In Section 2, the basic theory for the polarization characteristic of the proposed switch is presented by using the matrix multiplication method. In Section 3, the corresponding numerical simulation results for different splitter ratios and polarization states are presented. In Section 4, the analysis is verified through an experiment. In Section 5, some experimental measurements of the laser-induced damage threshold are discussed and the potential applications of the technology, especially in the Q-switched all-solid-state high power laser, are outlined. Finally, in Section 6, the conclusions are drawn from the present study.

2. Theoretical analysis for electro-optic switch

2.1. Electro-optic Q-switch

The electro-optic Q-switch is a key component for generating nanosecond-to-subpicosecond laser pulses. PLZT or PMNT is a high quadratic electro-optic material and may be considered as the electrically controllable phase retarder in the Q-switch as shown in Fig. 1. The applied electric field causes a change in the optical anisotropy of the birefringent ceramic characterized by two orthogonal directions (fast and slow axes which are parallel and perpendicular to the applied field) with different indices of refraction. An incident plane polarized beam (at α with respect to the applied electric field) will split into two components travelling at different velocities, corresponding to the more commonly employed half-wave light intensity retardation. At the output end, the other polarizer stands with a $\pi/2$ angle with respect to the incident polarized direction.

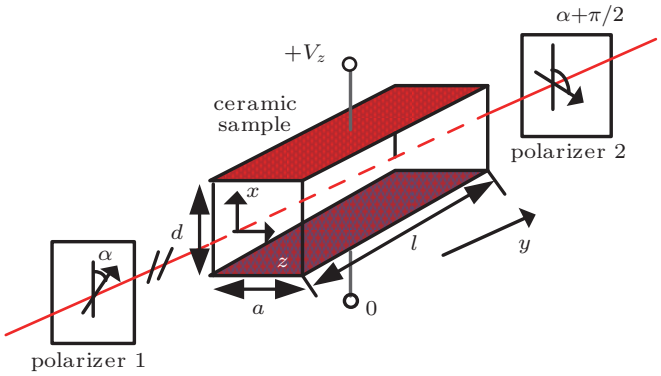


Fig. 1. (color online) Schematic of a Q-switch design with quadratic electro-optic ceramic.

The phase retardation contributed by the PLZT/PMNT ceramic is given by[13,14]

$$\varphi = \frac{\pi n^3}{\lambda}\gamma_{\text{eff}} l \left(\frac{V_z}{d}\right)^2, \tag{1}$$

where V_z is the applied voltage, l is the length of the ceramic along the light transmission direction, d is the distance between two electrodes along the x axis, n is the refractive index of the ceramic, and γ_{eff} is the corresponding effective electro-optic coefficient. Thinner and longer materials are required to reduce the half-wave voltage. The Jones matrix is used to express the output intensity. When the principle axis is parallel to the x axis, the electrical-controlled birefringent material can be described as follows:

$$\boldsymbol{J}_{\text{Sample}} = \begin{bmatrix} \cos\dfrac{\varphi}{2} + \mathrm{j}\sin\dfrac{\varphi}{2} & 0 \\ 0 & \cos\dfrac{\varphi}{2} - \mathrm{j}\sin\dfrac{\varphi}{2} \end{bmatrix}. \tag{2}$$

The corresponding matrices for the linearly polarized beam produced by polarizer 1 (P1) and polarizer 2 (P2) may be written respectively as

$$\boldsymbol{J}_{\text{P1}} = \begin{bmatrix} \cos\alpha \\ \sin\alpha \end{bmatrix}, \tag{3a}$$

$$\boldsymbol{J}_{\text{P2}} = \begin{bmatrix} \cos^2\left(\alpha+\dfrac{\pi}{2}\right) & -\dfrac{1}{2}\sin 2\left(\alpha+\dfrac{\pi}{2}\right) \\ -\dfrac{1}{2}\sin 2\left(\alpha+\dfrac{\pi}{2}\right) & \cos^2\left(\alpha+\dfrac{\pi}{2}\right) \end{bmatrix}. \tag{3b}$$

Then the output beam matrix and intensity (I_0) is

$$I_{\text{out}} = |\boldsymbol{J}_{\text{out}}|^2 = \left|\boldsymbol{J}_2 \boldsymbol{J}_{\text{Sample}} \boldsymbol{J}_{\text{P}}\right| = \sin^2 2\alpha \sin^2\frac{\varphi}{2}. \tag{4}$$

It is obvious that the switch output intensity is closely related to the input polarization state (i.e., α). This Q-switch structure is polarization-dependent. Figure 2 shows that the intensity changes as a function of phase retarder φ and input polarization angle α of the polarized beam.

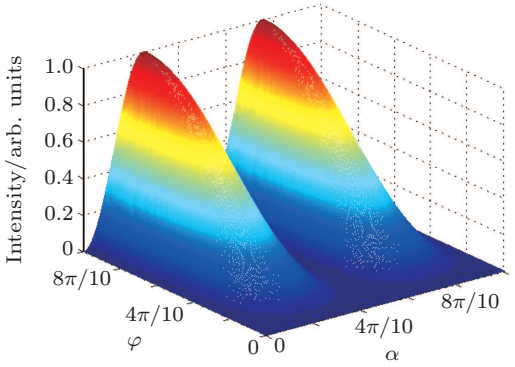


Fig. 2. (color online) Intensity changes with phase change and polarization angle.

2.2. Theoretical design of a polarization-independent electro-optic switch

Polarization-independence is very important for a laser system and may exempt some complex optic or electric technology. In this subsection, a novel high-power polarization-independent electro-optic switch based on a reciprocal structure Sagnac interferometer and a transparent quadratic electro-optic ceramic is proposed and analyzed in detail as shown in Fig. 3(a). The incident polarized beam has an angle of α relative to the x axis. A beam splitter (BS) and three mirrors (M1, M2, M3) are used to build the Sagnac interferometer that has good reciprocity for clockwise and counter-clockwise polarized light. Two half-wave plates (HP1 and HP2) with a 45° angle between their principal axis directions are added to the Sagnac loop to keep the incident clockwise and counter-clockwise polarized beams on the electrically controllable birefringence ceramic orthogonal. The principal axis direction of one half-wave plate has an angle of θ relative to the x axis, while the other half plate has an angle of θ +45° respect to the x axis. When the orthogonal polarized beam is incident on the electro-optic birefringence ceramic sample, a phase difference is observed between the two polarized beams because of the difference between their quadratic electro-optic coefficients,[9] as shown in Fig. 3(b).

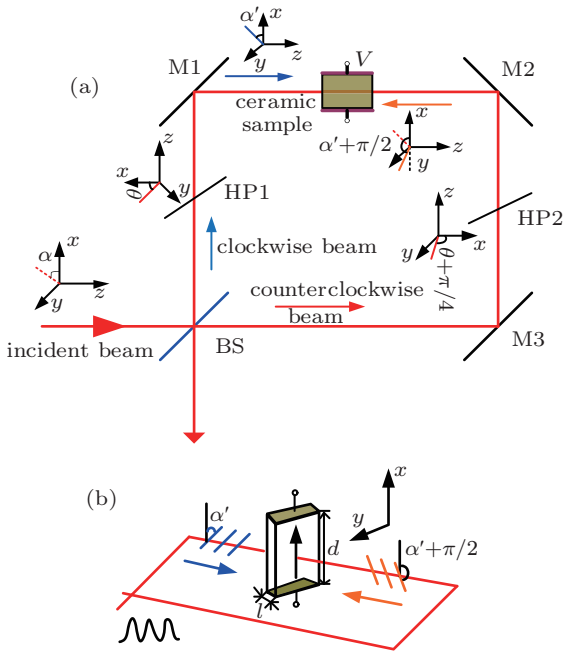


Fig. 3. (color online) (a) Theoretical scheme of the polarization-independent switch. (b) Phase difference between two polarized beams.

If we ignore the intensity losses due to the wave plates and beam splitter absorption, and assume that all reflections will lead to a π phase difference and the angle between the main axis of HP1 and the x axis is θ, then the Jones matrices for the components may be written as

$$\boldsymbol{J}_{\mathrm{M,BSr}} = \begin{bmatrix} 1 & 0 \\ 0 & \exp(\mathrm{j}\pi) \end{bmatrix}, \tag{5}$$

$$\boldsymbol{J}_{\mathrm{HP1}} = \mathrm{j}\begin{bmatrix} \cos 2\theta & \sin 2\theta \\ \sin 2\theta & -\cos 2\theta \end{bmatrix}, \tag{6a}$$

$$\boldsymbol{J}_{\mathrm{HP2}} = \mathrm{j}\begin{bmatrix} \cos 2(\theta+\pi/4) & \sin 2(\theta+\pi/4) \\ \sin 2(\theta+\pi/4) & -\cos 2(\theta+\pi/4) \end{bmatrix}. \tag{6b}$$

By the matrix multiplication method, the transmission matrices for the clockwise (cw) and counter-clockwise (ccw) polarized beams are obtained as

$$\begin{aligned} \boldsymbol{J}_{\mathrm{cw}} &= \boldsymbol{J}_{\mathrm{BS}}\boldsymbol{J}_{\mathrm{M3}}\boldsymbol{J}_{\mathrm{HP2}}\boldsymbol{J}_{\mathrm{M2}}\boldsymbol{J}_{\mathrm{PMNT}}\boldsymbol{J}_{\mathrm{M1}}\boldsymbol{J}_{\mathrm{HP1}}\boldsymbol{J}_{\mathrm{BS}}\boldsymbol{J}_{\mathrm{P}} \\ &= -\begin{bmatrix} -\sin 2\theta\cos(2\theta+\alpha)\exp\left(\mathrm{j}\frac{\varphi}{2}\right)+\cos 2\theta\sin(2\theta+\alpha)\exp\left(-\mathrm{j}\frac{\varphi}{2}\right) \\ \cos 2\theta\cos(2\theta+\alpha)\exp\left(\mathrm{j}\frac{\varphi}{2}\right)+\sin 2\theta\sin(2\theta+\alpha)\exp\left(-\mathrm{j}\frac{\varphi}{2}\right) \end{bmatrix}, \end{aligned} \tag{7a}$$

$$\begin{aligned} \boldsymbol{J}_{\mathrm{ccw}} &= \boldsymbol{J}_{\mathrm{BS}}\boldsymbol{J}_{\mathrm{HP1}}\boldsymbol{J}_{\mathrm{M1}}\boldsymbol{J}_{\mathrm{PMNT}}\boldsymbol{J}_{\mathrm{M2}}\boldsymbol{J}_{\mathrm{HP2}}\boldsymbol{J}_{\mathrm{M3}}\boldsymbol{J}_{\mathrm{P}} \\ &= \begin{bmatrix} -\sin 2\theta\cos(2\theta+\alpha)\exp\left(-\mathrm{j}\frac{\varphi}{2}\right)+\cos 2\theta\sin(2\theta+\alpha)\exp\left(\mathrm{j}\frac{\varphi}{2}\right) \\ \cos 2\theta\cos(2\theta+\alpha)\exp\left(-\mathrm{j}\frac{\varphi}{2}\right)+\sin 2\theta\sin(2\theta+\alpha)\exp\left(\mathrm{j}\frac{\varphi}{2}\right) \end{bmatrix}. \end{aligned} \tag{7b}$$

The output is a linearly polarized beam that has a 4θ deflection angle with respect to the incident light. When the principle axis of HP1 is designed to be parallel to the applied voltage (i.e., the x axis), the output light intensity becomes independent of incident angle α and may be described as

$$\begin{aligned} I_{\text{out}} &= |\boldsymbol{J}_{\text{ccw}} + \boldsymbol{J}_{\text{cw}}|^2 \\ &= \left| 2\text{j}\sin\frac{\varphi}{2}\begin{bmatrix}\sin(4\theta+\alpha)\\ \cos(4\theta+\alpha)\end{bmatrix}\right|^2 \propto \sin^2\frac{\varphi}{2}. \end{aligned} \tag{8}$$

Apparently the output intensity from the Sagnac interferometer is associated only with the phase difference $\varphi = 2\pi n_0^3 L\gamma_{\text{eff}}(V_z/d)2\lambda$, and independent of the polarization angle α of the incident light. This characteristic is unique for the proposed electro-optic switch type.

Based on the above theoretical analysis, some numerical simulation results are given to analyze the effect of each component on the characteristic of the proposed switch. A new component of PMNT ceramic is used as an electrically controllable phase retarder and the corresponding parameters are $l = 2$ mm, $a = 10$ mm, and $d = 1$ mm. The effective quadratic electro-optic coefficient γ_{eff} is 28×10^{-16} m^2/V^2 from the measurement in Ref. [11], which describes the birefringence ability. The refractive index of the PMNT ceramic is $n = 2.45$. Figure 4 illustrates the numerical simulation results based on Eqs. (1) and (8). With increasing applied voltage, the switch characteristic is obvious and the ON/OFF voltage is about 305 V. The incident angle α has a slight effect on the performance of the switch. If the amplitude components along the x and y axes can be written as A_x and $A_y\exp(\text{j}\Delta\varphi)$, respectively, a Poincare sphere coordinate can be used to describe the output polarization state, where two parameters, i.e., the azimuthal angle ($\omega = 1/2\arcsin(2A_xA_y\sin\Delta\varphi)$) and the ellipticity ($\psi = \tan(2A_xA_y)\cos\Delta\varphi$), are introduced to represent all polarization states,[15] as demonstrated in Fig. 5. The polarized light is right-handed when $\omega > 0$, and left-handed when $\omega < 0$. When $\omega = 0$, the input light and output light are located at the equator and linearly polarized.

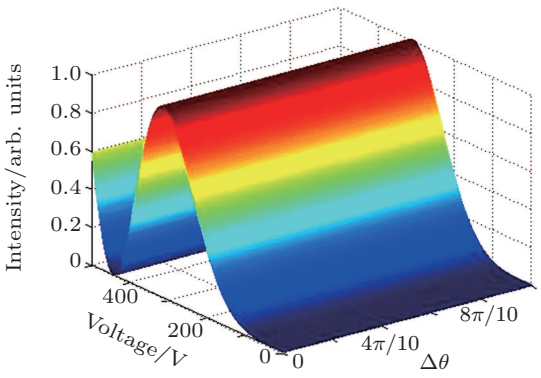


Fig. 4. (color online) Output intensity versus applied voltage.

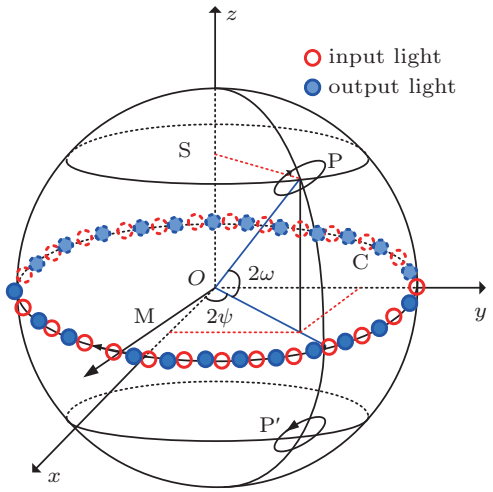


Fig. 5. (color online) Description of polarization states on the Poincare sphere.

In our design, two half-wave plates are inserted into the Sagnac interferometer to maintain the polarization angle $\theta = \pi/4$ strictly for clockwise light and counter-clockwise light in which they are orthogonal on the face of the electrically controllable birefringence ceramic sample. However, some angle difference $\Delta\theta = \theta - \pi/4$ will be introduced to degrade the polarization-independent performance, which is shown in Fig. 6, where the incident light is parallel to the x axis, i.e., $\alpha = 0$. The switch will present polarization-independent characteristics only when the angle $\Delta\theta$ is an even multiple of $\pi/4$ (i.e., $\Delta\theta = 2\times\pi/4,\ 4\times\pi/4,\ldots$). For odd multiples of $\pi/4$ ($\Delta\theta = 1\times\pi/4,\ 3\times\pi/4,\ldots$), the switch characteristic will disappear with increasing applied voltage. The extinction ratio in this case will be a sine function of the angle difference $\Delta\theta$.

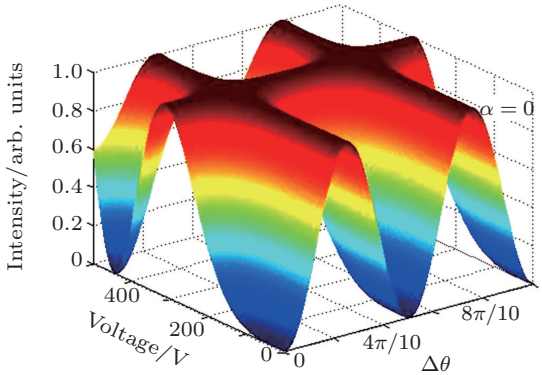


Fig. 6. (color online) Output intensity versus applied voltage with various angle difference $\Delta\theta$.

The effect of the incident light polarization state on the switch performance is also analyzed and simulated as shown in Fig. 7. When the angle difference $\Delta\theta = \pi/4$ and $\alpha = \pi/4$, the switch shows good switching characteristics by changing the applied voltage. Therefore, maintaining the polarization angle $\theta = \pi/4$ is an important condition in the proposed polarization-independent structure. In a practical experimental

setup, a very small angle difference $\Delta\theta$ may occur. In the following section, some analyses are carried out. When a small $\Delta\theta$ is introduced, equation (8) may be rewritten as

$$\begin{aligned} I_{\text{out}} &= |\boldsymbol{J}_{\text{ccw}} + \boldsymbol{J}_{\text{cw}}|^2 \\ &= \left| 2 \begin{bmatrix} -\sin 2\Delta\theta \cos\alpha \cos\dfrac{\varphi}{2} + \mathrm{j}\left[\sin(4\theta+\alpha+\Delta\theta)\right]\sin\dfrac{\varphi}{2} \\ \mathrm{j}\left[\cos(4\theta+\alpha+\Delta\theta)\right]\sin\dfrac{\varphi}{2} \end{bmatrix} \right|^2 \\ &\propto \sin^2(2\Delta\theta)\cos^2\alpha\cos^2\frac{\varphi}{2} + \sin^2\frac{\varphi}{2}. \end{aligned} \tag{9}$$

A real part in the Jones matrix comes out. When $\Delta\theta = \pi/10$, different polarization incident beams will induce different output extinction ratios; the corresponding simulation results are shown in Fig. 8. The intensity of "ON" switch state is not influenced, while the intensity of "OFF" state changes from $\alpha = 0$ to $\alpha = \pi/2$. The ratio reaches an ideal value at the point $\alpha = \pi/2$ and the output ratio keeps a level greater than 30 dB. Besides, the effect of $\Delta\theta$ on the switch performance is simulated. When $\Delta\theta = 1^\circ$, 2°, 5°, and 10°, the corresponding output extinction ratios decline from 29 dB to 23 dB, 15.2 dB, and 9.3 dB, respectively. Fortunately, the $\Delta\theta = 1^\circ$ deviation is easy to control and an extinction ratio larger than 29 dB can be obtained in the experiment.

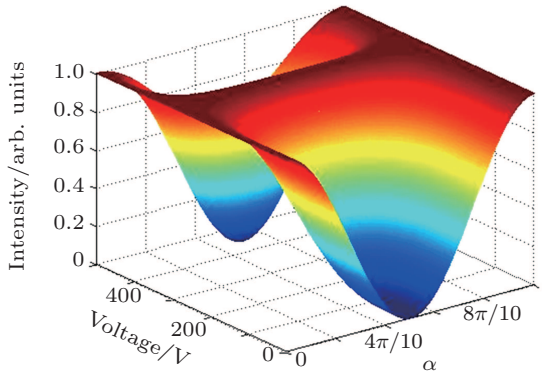


Fig. 7. (color online) Output intensity versus applied voltage for parallel polarized intersectional light (i.e., $\Delta\theta = \pi/4$).

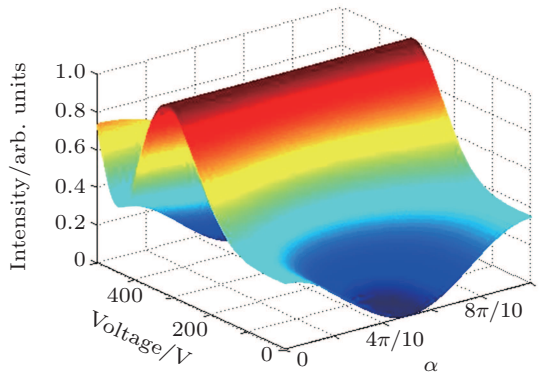


Fig. 8. (color online) Effect of angle $\Delta\theta = \pi/10$ on the performance of the switch.

The Jones matrix above shows that the output light is elliptically polarized. Thus, a Poincare sphere coordinate is used to illuminate the change in the polarization state. When $\Delta\theta = 1^\circ$, ω ranges from 0 to 8.3843×10^{-13}, and ψ difference ranges from -1.5573 to 1.5573; when $\Delta\theta = \pi/10$, the corresponding ω ranges from 0 to 1.4121×10^{-11}, and ψ changes from -1.5574 to 1.5574. The term ω is obviously so small that the approximately linear polarization vector of the output beam remains at the equator. Therefore, the angle $\Delta\theta$ has a slight effect on the polarization state of the output beam, but has a large effect on the extinction ratio.

In our designed structure, various incident angles on the BS or mirror lead to different phase shifts for the reflection beam, i.e., the reflection mirror cannot exactly generate a π-phase shift. We assume that this additional phase shift is β and the corresponding Jones matrix is

$$\boldsymbol{J}'_{\text{M}} = \begin{bmatrix} 1 & 0 \\ 0 & \exp(\mathrm{j}\beta) \end{bmatrix}. \tag{10}$$

Using the matrix manipulation, the output intensity is expressed as

$$\begin{aligned} I_{\text{out}} &= |\boldsymbol{J}_{\text{out}}|^2 \\ &= \left| \exp(\mathrm{j}\frac{\varphi}{2}) + \exp\left(-\mathrm{j}\frac{\varphi}{2} + \mathrm{j}\beta\right) \begin{bmatrix} \sin(4\theta+\alpha) \\ -\cos(4\theta+\alpha) \end{bmatrix} \right|^2 \\ &\propto \sin^2\frac{\varphi-\beta}{2}. \end{aligned} \tag{11}$$

Figure 9 shows the simulation results obtained for different phase shift β. The corresponding ON/OFF voltage increases with phase shift β increasing from 0 to π. In order to solve this problem, the phase shift must be compensated for by the modulation voltage applied to the ceramic sample in the practical application.

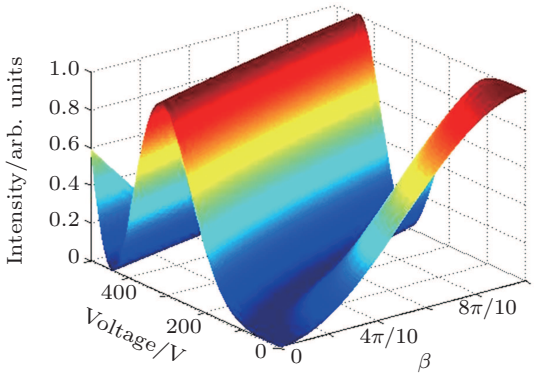


Fig. 9. (color online) Intensity versus applied voltage with different additional phase shift β.

The splitting ratio of the BS, which cannot be exactly 1:1 because of differences in wavelength and power, is another factor influencing the output intensity. If the splitting ratio of the BS is $\eta : 1$, the corresponding output intensity is

$$I_{\text{out}} = |\boldsymbol{J}_{\text{out}}|^2$$

$$= \left| \begin{bmatrix} (1-\eta)\sin\alpha\cos\dfrac{\varphi}{2} + \mathrm{j}(\eta+1)\sin\dfrac{\varphi}{2}\sin(4\theta+\alpha) \\ (1-\eta)\cos\alpha\cos\dfrac{\varphi}{2} - \mathrm{j}(\eta+1)\sin\dfrac{\varphi}{2}\cos(4\theta+\alpha) \end{bmatrix} \right|^2$$
$$\propto \left(\eta^4 + 1 - 2\eta^2\cos\varphi\right)/\left(\eta^2+1\right)^2. \quad (12)$$

Figure 10 demonstrates the numerical simulation results for different splitting ratios and polarization states. When the splitting ratios are 50:50, 51:49, 55:45, and 60:40, the switch extinction ratios are about 60 dB, 34.2 dB, 20.8 dB, and 15.6 dB, respectively. The switch performance shows significant effect with the asymmetric increase of the splitting ratio. The intensities of ON/OFF states both change. The polarization state in the Poincare sphere coordinate shows that the output light is elliptically polarized, as shown in Fig. 10(b).

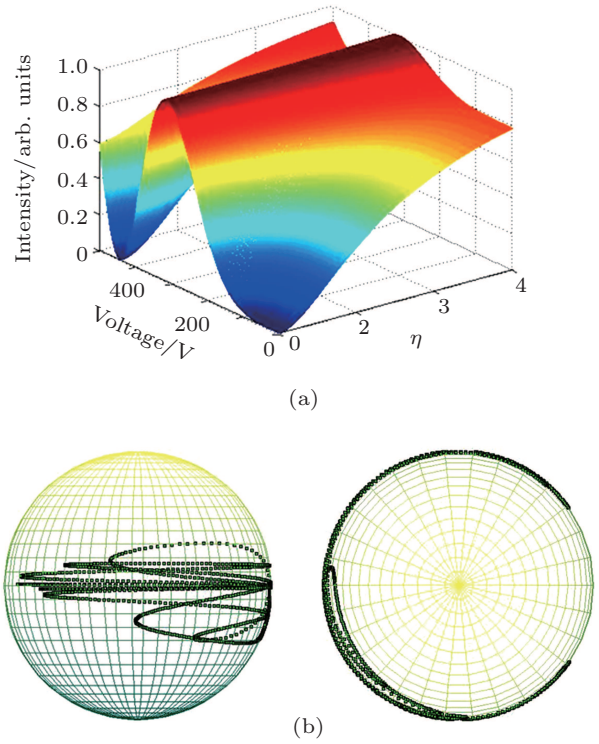


Fig. 10. (color online) (a) Output intensity with different splitting ratios. (b) Polarization states in the Poincare sphere coordinate when $\eta = 1.1$.

3. Experimental setup

We design an experimental setup to verify the analysis described above, as shown in Fig. 11. The key component in the system is an electro-optic phase retarder. The electro-optic ceramic has a large refractive index and must be polished to reduce the transmission loss. A polarized incident beam with a narrow-linewidth 785 nm from an external cavity diode laser (ECDL) is incident on a polarized beam splitter (PBS) to obtain the linearly polarized light. The direction of the linearly polarized light can be changed by adjusting a half-wave plate (HP1). The Sagnac interferometer is composed of one beam splitter (BS), three total reflective mirrors, two half-wave plates (HP2 and HP3), and the PMNT phase retarder onto which Ti/Au electrodes are sputtered on the top and bottom surfaces. The BS is replaced by a non-polarizing beam splitter (NPBS) to avoid the interference between the two faces of the BS, it has a split ratio of 50:50. The optical field is set to maintain an incident angle of 45° when inputted on all optical components. A photoconductive detector (PD) is employed to obtain the output intensity from the switch.

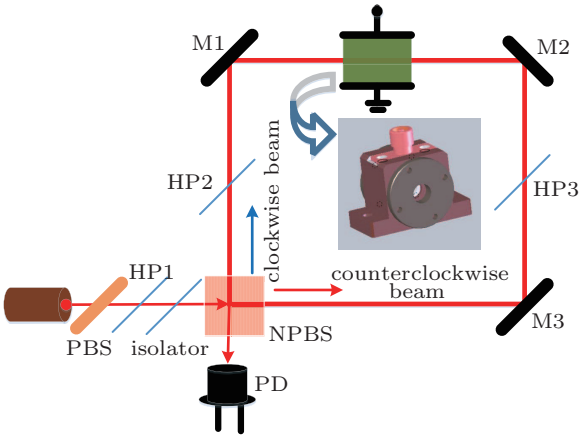


Fig. 11. (color online) Schematic diagram of the experimental setup for the polarization-independent electro-optic switch.

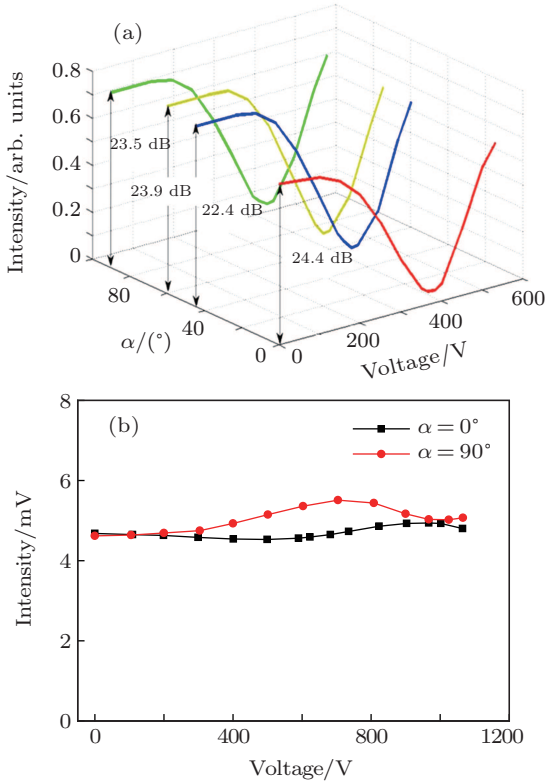


Fig. 12. (color online) (a) Switch performance for different incident linearly polarized beams. (b) Output intensity versus applied voltage when $\Delta\theta = \pi/4$ with different incident angles.

Figure 12(a) shows the experimental measurement results for different linearly polarized beams obtained by adjusting HP1. The results show that different linear polarizations have little effect on the switch performance and the extinction ratios are larger than 23 dB, which is 2 dB higher than the results in

Ref. [12] and agrees with the theoretical analysis presented earlier. When $\Delta\theta = \pi/4$, the switch characteristic will disappear with increasing applied voltage, as shown in Fig. 12(b). The switch response time is also measured, and the results are shown in Fig. 13. The response time of the switch is about 180 ns, and this speed may be improved by reducing the spacing between the electrodes.

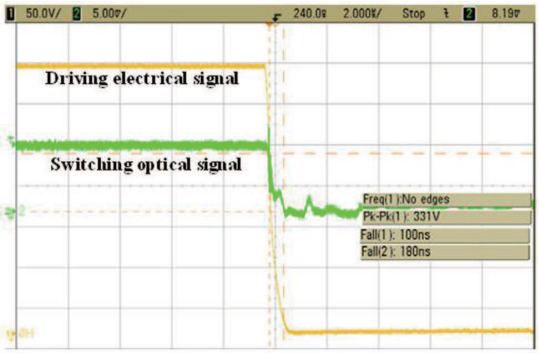


Fig. 13. (color online) Response time of the polarization-independent modulator.

4. Discussion and applications

4.1. Laser-induced damage threshold

For a high-power laser system, the laser-induced damage threshold is a very important parameter that directly affects the component lifetime. Because the PBS, mirror, and HP are very mature components in laser systems, we focus on analyzing the laser damage threshold of the quadratic electro-optic ceramic in this subsection. In our experiment, the samples are polished and the surface waviness is maintained within 10 nm. Damage morphologies on the ceramic sample surface induced by nanosecond pulses at the wavelength of 1064 nm are recorded; here, the pulses are nearly Gaussian beams and the pulse duration is 12 ns. According to the one-on-one regime of ISO 11254-1,[16,17] twenty sites for each energy density are tested. Error analysis of pulse energies, spot sizes, and so on yields an error budget of damage probability of about 15%. The damage probability is observed online, and the pulse powers are adjusted to suitable levels. Damage morphologies induced by different energy levels are also observed by a microscope (VHX-700F company KEYENCE CORPORATION) with a very incident angle. Figure 14 shows the damage morphologies observed under a magnification of 50.

The damage probability is 100% when the irradiation energy is 17.6 J/cm^2 or above. With the energy declining, the damage probability reduces to 80% when the energy is 14 J/cm^2. When the energy is 5.7 J/cm^2, the ceramic shows no damage spot on the surface. According to linear fitting, the laser-induced damage threshold of the ceramic is 5.79 J/cm^2. By contrast, the lithium tantalite ($LiTaO_3$) and other widely-used crystals all have a value around 1.4 J/cm^2.

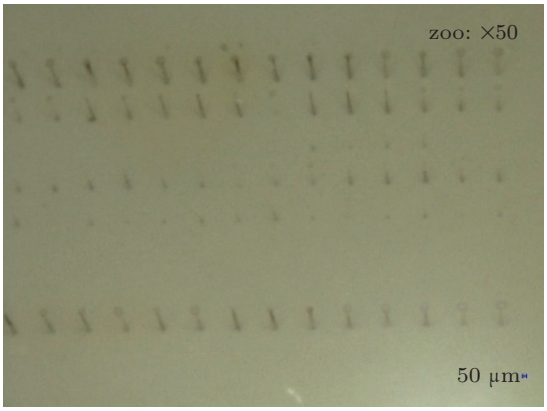


Fig. 14. (color online) Damage morphologies obtained when the samples are irradiated by nanosecond pulses of different energy levels.

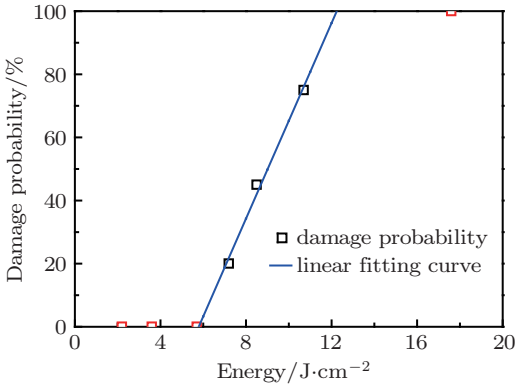


Fig. 15. (color online) Laser-induced damage threshold of ceramic.

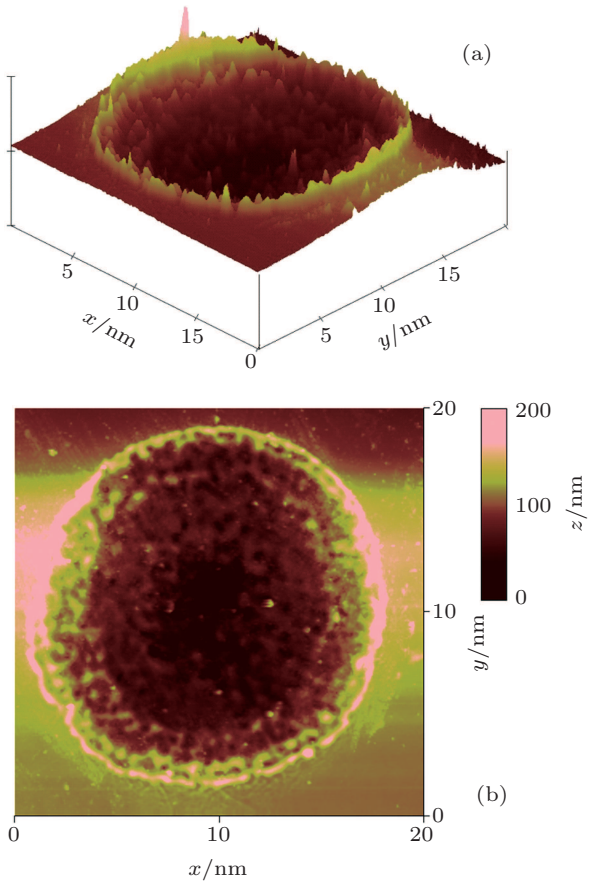


Fig. 16. (color online) AFM images of the stereoscopic damage morphology.

Figure 15 shows the result of damage threshold linear fitting. A total of 20 sites per energy level and 9 energy levels are used in this study.

Variations of damage spot diameter with irradiation energy are analyzed. Variations of damage depth with damage spot diameter and the damage morphology in the ceramic are also detected and recorded. Small damage spots are observed by atomic force microscopy, and the images obtained are presented in Fig. 16. The laser irradiation causes a damage spot with a diameter of 200 nm and a depth of 90 nm. Figure 16 shows that the depth of the damage spot has a Gaussian-like distribution along the diameter direction, and is nearly in conformity with the pulse energy distribution.

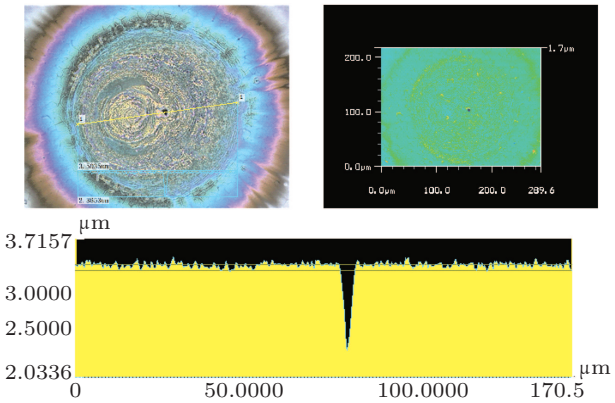


Fig. 17. (color online) Damage and defect morphology.

A damage dot caused by defects in the ceramic is presented in Fig. 17; here, the irradiation energy is 17.8 J/cm^2, and the dot depth is 1 μm.

The grain boundary and porosity in polycrystalline ceramic are known to influence transmittance. Lengthening the holding time and two-stage sintering the conventional starting materials lead to the decrease of the ultimate residual porosity, improve the density and transmittance, and yield a pure phase perovskite structure. Over 10% La doping can yield the pyrochlore phase and affect the transmissivity of the material. Thus, La doping must be controlled to an appropriate proportion. The electric domain size is another key factor affecting the transmittance and electro-optic performance: this factor also depends on the Pt and La contents. During cooling, the furnace is partially opened to achieve different cooling speeds and obtain smaller grains. All these steps will be taken into consideration in future studies to raise the laser-induced damage threshold.

4.2. Applications in high-power laser systems

The polarization-independent switch can be considered as a Q-switch optical intensity modulator for intracavity or external cavity laser modulation[18] as shown in Fig. 18. The remarkable advantages for Q-switch optical intensity modulators should be noticed which include high laser damage threshold and large component size because of the transparent electro-optic ceramic used. The polarization-independent switch can also be employed in satellite lidars, which are now beginning to provide new capabilities for global atmospheric sensing from space. The cloud aerosol lidar and infrared pathfinder satellite observation (CALIPSO)[19] mission, for example, uses a dual-wavelength lidar system. Figure 19 shows that the system operates at 1064 nm and 532 nm to measure the coverage, depth, and composition of atmospheric clouds and aerosols. The polarization-independent switch has promising applications in lasers, especially in high-power laser systems.

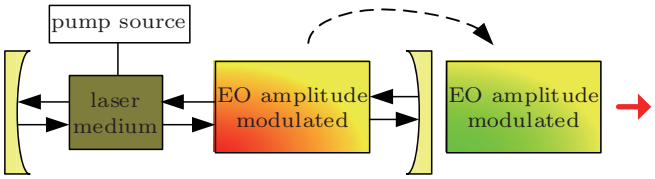


Fig. 18. (color online) Intracavity and extracavity beam control in high power ultra-short pulse laser application.

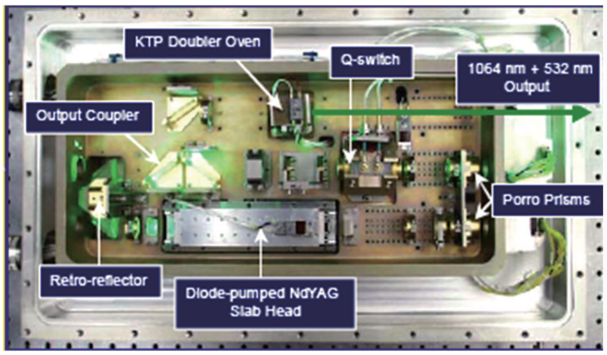


Fig. 19. (color online) CALIPSO laser transmitter.

5. Conclusion

A novel high-power polarization-independent electro-optic switch technology based on a reciprocal structure Sagnac interferometer and a transparent quadratic electro-optic ceramic is investigated. The polarization-independent characteristic of the device and the output optical beam induced by the controllable electric field are analyzed theoretically, simulated numerically, and implemented experimentally. Research shows that the experimental results in the free space Sagnac structure are accordant very well with the theoretical analysis. Some potential applications of the high-power laser system for polarization-independent modulation are discussed. The laser-induced damage threshold of the ceramic is also measured in this study. Damage morphologies obtained under different powers and different pulse widths are shown and some

techniques, such as two-step sintering and lengthening holding time, are speculated to increase the laser-induced damage threshold.

Acknowledgment

We thank Prof. Li Guorong and Prof. He Xiyun for their support.

References

[1] Li R, Wang C, Su G Z, Zhang K, Tang L and Li C 2007 *Science & Technology Review* **25** 58
[2] Anthony W Y, Michael A K, David J H, James B A and Sun X 2010 *Proc. SPIE* **7578** 757802
[3] Wang Y H, Wang J F, Jiang Y E, Bao Y, Li X C and Lin Z Q 2008 *Chin. Opt. Lett.* **6** 841
[4] http://www.photoptech.com/main/products_gx/Electro-Optic%20Crystals.php.
[5] Qiao L, Ye Q, Gan J L, Cai H W and Qu R H 2011 *Opt. Commun.* **284** 3886
[6] Li K K 2002 *US Patent Application* 10/139857
[7] Kamzina L S, Ruan W, Li G, Zeng J and Ding A 2010 *Magnetism and Ferroelectricity* **52** 2142
[8] Jiang H, Zou Y, Ming H, Zhang X and Chen M Y 2004 *Proc. SPIE* **5644** 380
[9] Ye Q, Qiao L, Cai H W and Qu R H 2011 *Opt. Lett.* **36** 2453
[10] Ye Q, Qiao L, Gan J L, Cai H W and Qu R H 2010 *Opt. Lett.* **35** 4187
[11] Zhang X J, Ye Q, Cai H W and Qu R H 2013 *Chin. J. Lasers* **40** 0708004 (in Chinese)
[12] Zhang X J, Ye Q, Cai H W and Qu R H 2014 *Opt. Laser Tech.* **57** 5
[13] James A T 1998 *Optical Phased Array Beam Deflection Using Lead Lanthanum Zirconate Titanate* (Ph. D Dissertation) (San Diego: University of California)
[14] Max B and Emil W 2001 *Principle of Optics* (7th Edn.) (New York: World Publishing Corporation)
[15] Theocaris P S and Gdoutos E E 1979 *Matrix Theory of Photoelasticity* (Germany: Springer)
[16] Yan L, Wei C Y and Li D W 2012 *Appl. Opt.* **51** 3243
[17] Louchev O A, Hatano H, Wada S and Kitamura K 2013 *Appl. Phys. Lett.* **103** 091114
[18] Sato H and Toda K 1977 *Appl. Opt.* **16** 1280
[19] Winker D, Vaughan M and Hunt B 2006 *Proc. SPIE* **6409** 640902